ACS Sustainable Chemistry & Engineering

Research Article

pubs.acs.org/journal/ascecg

# Recovery of Lithium from Wastewater Using Development of Li Ion-Imprinted Polymers

Xubiao Luo,[†] Bin Guo,[†] Jinming Luo,[‡] Fang Deng,[†] Siyu Zhang,[§] Shenglian Luo,*[,†] and John Crittenden*[,∥]

[†]Key Laboratory of Jiangxi Province for Persistent Pollutants Control and Resources Recycle, Nanchang Hangkong University, Nanchang 330063, People's Republic of China

[‡]Key Laboratory of Drinking Water Science and Technology, Research Center for Eco-Environmental Sciences, Chinese Academy of Sciences, Beijing 100085, People's Republic of China

[§]State Key Lab of Urban and Regional Ecology, Research Center for Eco-Environmental Sciences, Chinese Academy of Sciences, Beijing 100085, People's Republic of China

[∥]School of Civil and Environmental Engineering and the Brook Byer Institute for Sustainable Systems, Georgia Institute of Technology, 828 West Peachtree Street, Atlanta, Georgia 30332, United States

Supporting Information

**ABSTRACT:** Recycling lithium from waste lithium batteries is a growing problem, and new technologies are needed to recover the lithium. Currently, there is a lack of highly selective adsorption/ion exchange materials that can be used to recover lithium. We have developed a magnetic lithium ion-imprinted polymer ($Fe_3O_4$@$SiO_2$@IIP) by using novel crown ether. The $Fe_3O_4$@$SiO_2$@IIP has been synthesized by a surface imprinting technique using our newly synthesized 2-(allyloxy) methyl-12-crown-4 as a functional monomer. The $Fe_3O_4$@$SiO_2$@IIP was analyzed by Fourier infrared spectroscopy (FT-IR), scanning electron microscopy (SEM), and X-ray diffraction (XRD). The optimum pH for adsorption is 6. $Fe_3O_4$@$SiO_2$@IIP shows fast adsorption kinetics for lithium ions (10 min to reach complete equilibrium), and the adsorption process obeys an external mass transfer model. Homogeneous binding sites are proved by the Langmuir isotherm, and the maximum adsorption capacity is 0.586 mmol/g. $Fe_3O_4$@$SiO_2$@IIP has excellent selectivity for Li(I) because the selectivity separation factors of Li(I) with respect to Na(I), K(I), Cu(II), and Zn(II) are 50.88, 42.38, 22.5, and 22.2, respectively. The adsorption capacity of sorbent remained above 92% after five cycles. Fixed-bed column adsorption experiments indicate that the effective treatment volume was 140 bed volumes (BV) in the first run with a breakthrough of 10% of the inlet concentration for an inlet concentration of 0.5 mmol/L, and 110 BV was treated for the second run under identical conditions. We demonstrated that 89.8% of the lithium was recovered during bed regeneration using 0.5 mol/L HCl solution. $Fe_3O_4$@$SiO_2$@IIP also exhibited excellent removal efficiency for Li(I) in real wastewater, validating its great potential in advanced wastewater treatment. Accordingly, we have developed a new method for wastewater treatment that meets Li emission standards, and recovery of Li creates economic interest.

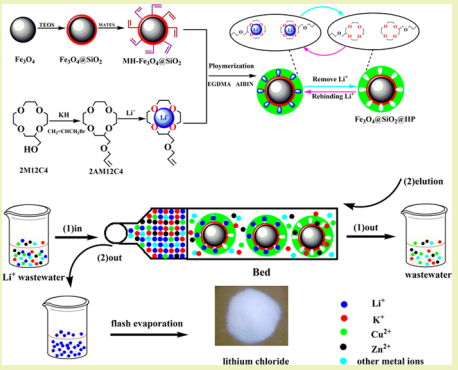


**KEYWORDS:** *$Fe_3O_4$@$SiO_2$@IIP, Wastewater, Lithium, Recovery, Crown ether*

## INTRODUCTION

Lithium ion batteries (LIBs) are extensively used as electrochemical power sources due to their advantages such as high cell voltage, high energy density, low self-discharge rate, and long storage life.[1,2] The annual global consumption of LIBs increased as high as 14.5% from 2006 to 2011, and the global consumption of LIBs reached $4.49 \times 10^9$ units in 2011.[3] Consequently, more consumption of LIBs implies more spent LIBs. In fact, it is evaluated that 200−500 MT of spent LIBs are annually produced.[4]

The research on recovery of LIBs has attracted great interest in recent years.[5−7] The hydrometallurgical process is a commercial method for recycling metals from spent LIBs.[3] In this method, the dismantled electrodes are dissolved in concentrated acids,[8] and then the dissolved metals can be recovered by extraction, precipitation. or electrodeposition.[9−11] The traditional pyrometallurgical method burns off all the organic electrolyte and binder, which makes it easier to recover valuable metals.[12] However, these processes can only recycle cobalt effectively, and hydrometallurgical and pyrometallurgical processes are not adaptable for lithium recycling.[13] Also, using these processes, lithium ions are usually discharged as waste,

Received: October 17, 2014
Revised: January 30, 2015
Published: February 9, 2015





DOI: 10.1021/sc500659h
ACS Sustainable Chem. Eng. 2015, 3, 460−467

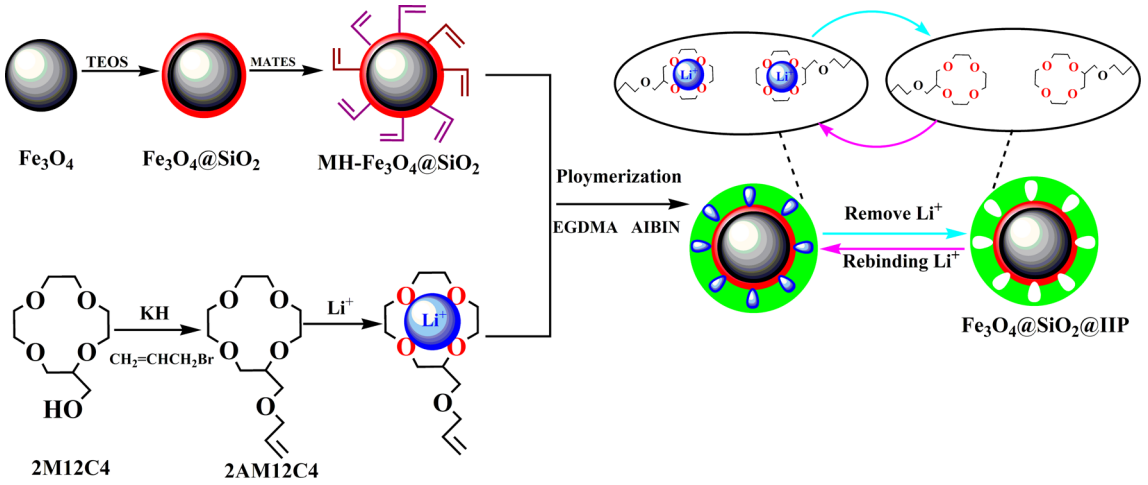


**Figure 1.** Synthesis route for $Fe_3O_4$@$SiO_2$@IIP.

which results in a significant waste of lithium resources. As far as human health is concerned, exposure to lithium ions may result in damage to the nervous system, kidneys, liver, brain, and cardiovascular and endocrine systems.[14−16] Consequently, it is important to remove and recycle lithium ions from industrial wastewater produced by spent lithium battery operations.

Research on lithium recovery has begun, but it is in its infancy. The utilization of sorption, nanofiltration, and electrolysis have been proposed.[13] Biological recovery of the $Li^+$ ion using various microorganisms is also possible according to Tsuruta.[17] The precipitation of Li using $CO_3^{2-}$ can be used to recover lithium from a relatively clean aqueous solution. Due to the large solubility product constant of lithium carbonate ($K_{sb}$ = 1.7 × $10^{-3}$ 25 °C), lithium ions cannot be completely precipitated. Adsorption is a cost-effective and environmentally friendly method for recovering lithium from aqueous solution.[18] However, most adsorbents are nonspecific, showing low selectivity toward a particular metal.[19] Therefore, it is important to exploit a new adsorbent for selective separation of Li from aqueous solution.

The ionic imprinting technique is an efficient method to prepare ion-imprinted polymers (IIPs) in which specific binding sites for the host molecules/ions are created by the addition and subsequent extraction of template molecules/ions. IIPs have promising prospects in the selective recovery of noble metals and heavy metals from aqueous solution.[20−22] Hoai et al. have synthesized porous adsorbent for selective recovery of copper ions using the ion-imprinting technique with methacrylic acid (MMA) and vinylpyridine (4-VP) as bifunctional ligands.[23] Li et al. developed an IIP to remove cadmium ions using a thiocyanato functional group as the complexing site for Cd.[24] In our previous work, $-NH_2$ and −SH functionalized IIPs were used to remove copper and lead ions from wastewater.[25,26] It is difficult to prepare lithium IIPs using coordination/complexation routes between functional monomers because lithium ions cannot combine in a stable fashion with the common functional monomers. Therefore, we had to design new functional monomers for the preparation of lithium IIPs.

Crown ethers (CEs) are very useful model compounds that possess a variety of chemical structures. Compared with the corresponding open chain analogues, CEs show higher selectivity for metal ions, and the complexes of CEs with metal ions are more stable, which is due to the so-called"macrocyclic effect".[27] In addition, the size of the crown ring and chelating ability of CEs can be adjusted by altering side chain groups or the number of ether groups or substituting the ether group −O− with −S− or −N− groups. There are only a few of reports on the preparation of IIPs using CEs.[28−30] Crown ethers have shown high selectivity for binding the target metal ions when the crown ethers have cavities with the appropriate size and have suitable functional and cross-linking monomers. Nevertheless, it is not easy to separate the IIPs rapidly and effectively from wastewater after treatment.

In the past decade, $Fe_3O_4$ nanoparticles have attracted much attention because of their superparamagnetism, low toxicity, high biocompatibility, and easy separation from a liquid system using a magnetic field.[31−34] When IIPs are impregnated with $Fe_3O_4$, they can be easily separated by the application of a magnetic field. Furthermore, the coating of silica on $Fe_3O_4$ can increase the high graft ratio (more hydroxyl group) and stability under acidic conditions.[26] Zhang et al. successfully prepared core−shell magnetic ion-imprinted polymers ($Fe_3O_4$@$SiO_2$@IIP) with silica-coated $Fe_3O_4$ as the core and IIPs as the shell.[35] $Fe_3O_4$@$SiO_2$@IIP exhibited good performance, such as good magnetism and thermal resistance, and high stability under acidic condition,

To the best of our knowledge, due to the similar size, 2-methylol-12-crown-4 (2M12M4C) can easily combine with lithium ions forming a stable complex. Nevertheless, without the double bond, 2M12M4C cannot be used as a functional monomer during polymerization. Therefore, we have successfully synthesized new crown ethers with a double bond as a functional monomer. On the basis of the new functional monomer, a novel magnetic ion-imprinted polymer with a core−shell structure ($Fe_3O_4$@$SiO_2$@IIP) was synthesized by a surface imprinting technique using 2-(allyloxy)methyl-12-crown-4 as the functional monomer, lithium ion as the template, and ethylene glycol dimethacrylate as the cross-linker. We utilize Fourier infrared spectroscopy (FT-IR), X-ray diffraction (XRD), and scanning and electron microscopy (SEM) to analyze the $Fe_3O_4$@$SiO_2$@IIP samples. We also determined the adsorption capacity and kinetics and applied $Fe_3O_4$@$SiO_2$@IIP as a selective sorbent for recycling $Li^+$ from LIB wastewater.


DOI: 10.1021/sc500659h
ACS Sustainable Chem. Eng. 2015, 3, 460−467

## MATERIALS AND METHODS

**Synthesis of Functional Monomer 2-(allyloxy)methyl-12-crown-4 (2AM12C4).** Sections S1 and S2 of the Supporting Information display the chemicals and characterization methods. A 30% potassium hydride dispersion in mineral oil (0.32 g, 9 mmol) was mixed with 2-methylol-12-crown-4 (2M12C4, 0.40g, 1.94 mmol) in DMF at room temperature for 30 min, and then allyl bromide (1.22 g, 10.1 mmol) was added. The above mixture was stirred overnight. The reaction was quenched with methanol, and then the methanol was evaporated under reduced pressure. The product was washed with water for three times (3 × 100 mL), and then was extracted with $CH_2Cl_2$, dried with $MgSO_4(s)$ and filtered. The solvent was removed using a rotary evaporator, and the residue was purified by column chromatography ($SiO_2$, hexane/EtOAc 1:2). The $^1H$ chemical shifts of this product for the $^1HNMR$ spectrum that is suspended in DMSO for which all six hydrogen atoms are deuterium (400 Hz, $\delta$/ppm) are 5.89−5.82 (m, 1H), 5.22 (d, $J$ = 15.6, 1H), 5.16 (d, $J$ = 26.8, 1H), 3.91 (d, $J$ = 5.2 2H), and 3.67−3.32 (m, 17H), respectively. The $^{13}C$ chemical shifts of this product for the $^{13}C$ NMR spectrum that is suspended in DMSO for which all 11 carbon atoms are deuterium (100 MHz, $\delta$/ppm) are 135.16, 116.23, 77.81, 71.25, 70.99, 70.37, 70.07, 69.98, 69.89, 69.70, and 69.38, respectively. These results demonstrate that the product is 2AM12C4.

**Preparation of Lithium Ion-Imprinted Polymer ($Fe_3O_4$@$SiO_2$@IIP).** The MH-$Fe_3O_4$@$SiO_2$ preparation is described in detail in section S3 of the Supporting Information. In brief, $Fe_3O_4$@$SiO_2$@IIP was prepared by surface-imprinted polymerization (Figure 1). 2AM12C4 (1.23g, 5.0 mmol), lithium chloride monohydrate (0.302 g, 5.0 mmol), and a mixture of methanol and DMF(1/2 v/v, 60 mL) were added into a three-neck round-bottomed flask (150 mL). The mixture was stirred for 30 min at room temperature to form a clear solution to which EGDMA (4.95 g, 25 mmol), AIBN (180 mg, 1.1 mmol), and MH-$Fe_3O_4$@$SiO_2$ (2.0 g) were added. After being purged with argon for 30 min, the reaction mixture was sealed and stirred in a water bath at 25 °C for 2 h for the self-assembly of the 2AM12C4 and lithium ion. The mixture was subject to reflux at 70 °C overnight with continuous stirring. The resulting polymer particles were collected by an external magnet, and they were washed three times with methanol. Then the particles were washed three times with 0.5 mol/L hydrochloric acid to remove the $Li^+$ ion, followed by thorough washing with distilled water until pH 7.

The nonimprinted polymer ($Fe_3O_4$@$SiO_2$@NIP) was prepared under identical conditions as $Fe_3O_4$@$SiO_2$@IIP except that lithium chloride monohydrate was not added.

**Batch Adsorption Experiments.** $Fe_3O_4$@$SiO_2$@IIP or $Fe_3O_4$@$SiO_2$@NIP (50 mg) were equilibrated with 50 mL of $Li^+$ solutions with different initial concentrations and pH at a constant temperature of 25 °C for 12 h. The pH of the aqueous solution was controlled by adding 0.1 mol/L HCl or 0.1 mol/L NaOH. After adsorption equilibration, the adsorbent was collected under an external magnetic field, and the concentration of $Li^+$ in the supernatant was determined by using flame atomic absorption spectrometry (FAAS). The amount of the $Li^+$ ion absorbed on $Fe_3O_4$@$SiO_2$@IIP or $Fe_3O_4$@$SiO_2$@NIP was calculated as follows

$$Q = \frac{(C_0 - C_e)V}{m}$$

where $Q$ is the adsorption capacity (mmol $g^{-1}$); $C_0$ and $C_e$ are the initial and equilibrium concentration of lithium ions (mmol $L^{-1}$), respectively; $m$ is the mass of polymers (g); and $V$ is the volume of $Li^+$ solution (L).

**$Li^+$ Adsorption−Desorption Studies.** The $Li^+$-adsorbed imprinted polymers were desorbed by using 0.5 mol/L HCl solution to release lithium ions. Regenerated $Fe_3O_4$@$SiO_2$@IIP was placed into the adsorption medium and mechanically stirred at room temperature for 2 h. The final $Li^+$ ion concentration in aqueous solution was determined as above. After that, the $Fe_3O_4$@$SiO_2$@IIP was separated and washed with distilled water and then dried in vacuum drying oven. In order to test the reusability of $Fe_3O_4$@$SiO_2$@IIP, the adsorption−desorption studies were repeated five times.

**Fixed-Bed Column Adsorption.** PVC column (15 mm in diameter and 60 mm in length) was used to conduct fixed-bed column experiments. A total of 1.5 mL of wet $Fe_3O_4$@$SiO_2$@IIP was packed within the column. Flow rate was controlled by a speed-adjustable peristaltic pump (QP−01, China). The superficial liquid velocity (SLV) was 1.2 m/h, and the empty bed contact time (EBCT) was 0.15 min. Wastewater with Li(I) concentrations of 0.5 mmol/L was used. The exhausted $Fe_3O_4$@$SiO_2$@IIP was regenerated using 0.5 mol/L HCl solution and a flow rate of 1.0 m/h.

## RESULTS AND DISCUSSION

**Characterization.** The FT-IR spectra of 2M12C4, 2AM12C4, and $Fe_3O_4$@$SiO_2$@IIP are shown in Figure 2.

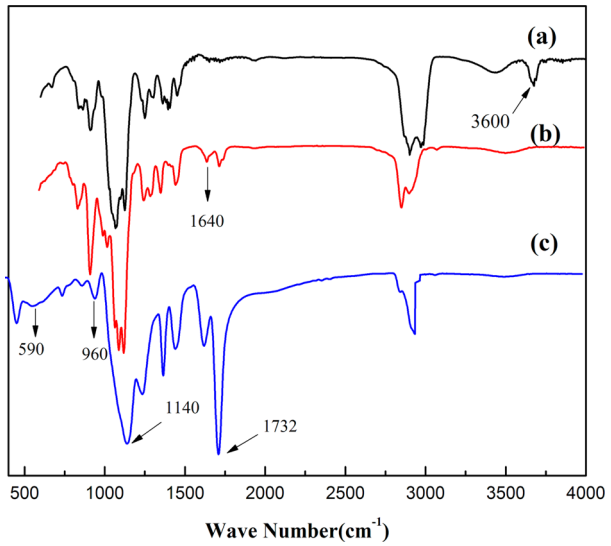


**Figure 2.** FT-IR spectra of 2M12C4 (a), 2AM12C4 (b), and $Fe_3O_4$@$SiO_2$@IIP (c).

The characteristic peak around 1140 $cm^{-1}$ corresponding to −O− stretching is observed in all samples. A characteristic peak of 2M12C4 was observed at about 3600 $cm^{-1}$ in Figure 2a, which is attributed to the −OH stretching vibration. The peak of −OH stretching vibration has disappeared in 2AM12C, and the IR absorption at around 1640 $cm^{-1}$ corresponds to the C═C stretching vibration (Figure 2b). These indicate that 2AM12C4 has been successfully synthesized. The peak at 590 $cm^{-1}$ indicates the Fe−O−Fe bond (Figure 2c). The absorption bands around 960 $cm^{-1}$ represent Si−O stretching vibrations. The peak at 1732 $cm^{-1}$ is due to the characteristic vibration frequencies of −C═O and the stretching vibrations of −O−. The results indicate that EGDMA reacted with 2AM12C4, and the imprinted polymer has been successfully synthesized on a $Fe_3O_4$@$SiO_2$ surface.

The morphologies of $Fe_3O_4$, $Fe_3O_4$@$SiO_2$, and $Fe_3O_4$@$SiO_2$@IIP were observed by scanning electron microscopy. As shown in Figure S1a of the Supporting Information, $Fe_3O_4$ is monodispersed and has a size of about 40 nm. After a layer of $SiO_2$ is immobilized on the $Fe_3O_4$ surface, the surface of $Fe_3O_4$@$SiO_2$ is uneven, and its size is about 200 nm (Figure S1b, Supporting Information). The average particle size of $Fe_3O_4$@$SiO_2$@IIP is 300 nm, which is larger than that of $Fe_3O_4$@$SiO_2$ (Figure S1c, Supporting Information). Thus, the imprinted shell is calculated to be about 50 nm.


DOI: 10.1021/sc500659h
ACS Sustainable Chem. Eng. 2015, 3, 460−467

As shown in Figure S2a of the Supporting Information, the diffraction peaks at $2\theta$ = 30.10°, 35.45 °, 43.08 °, 53.45 °, 56.98 °, and 62.57 ° are the reflection of (220), (311), (400), (422), (511), and (440) planes of the cubic $Fe_3O_4$ (JCPDS file No. 65-3107), respectively. The six peaks of the $Fe_3O_4$ in Figure S2b of the Supporting Information could be seen for $Fe_3O_4$@$SiO_2$, but the intensity decreases slightly. These results suggest that $SiO_2$ has been successfully coated on the surface of $Fe_3O_4$. The six peaks of the $Fe_3O_4$ in Figure S2c of the Supporting Information could be seen for synthesized $Fe_3O_4$@$SiO_2$@IIP, but the intensity decreases slightly. Moreover, after the coating of $SiO_2$ and polymerization, the peak positions do not change, indicating that the crystalline structure of $Fe_3O_4$ is maintained. This is in agreement with reported literature.[26] The above results may indicate that imprinted polymer is immobilized on the surface of $Fe_3O_4$@$SiO_2$ successfully.

**Adsorption Experiments.** *Effect of pH on Absorption Test.* pH was found to be one of the most critical parameters for adsorption of metals ion on the ion-imprinted polymer. The effect of pH values (1−9) on $Li^+$ ion adsorption on $Fe_3O_4$@$SiO_2$@IIP and $Fe_3O_4$@$SiO_2$@NIP was investigated, and the results were shown in Figure S3. The adsorption capacity of $Li^+$ on $Fe_3O_4$@$SiO_2$@IIP and $Fe_3O_4$@$SiO_2$@NIP increased with increasing the solution pH from 1.0 to 6.0 but decreased slightly from pH 6.0 to 9.0. When the pH is below pH 3.0, the adsorption capacity of $Li^+$ is low due to the protonation of the crown ether group; when the pH is higher than pH 3.0, high adsorption capacity of $Li^+$ is obtained as a result of deprotonation of the crown ether group. It can be inferred from the above results that the $Fe_3O_4$@$SiO_2$@IIP can be applied in a wide pH environment and solution pH should be adjusted to pH 6.0 for further studies.

*Absorption Capacity.* Adsorption equilibrium experiments were performed to determine the adsorption capacity of $Fe_3O_4$@$SiO_2$@IIP and $Fe_3O_4$@$SiO_2$@NIP for Li in a concentration range of 2.5−45 mmol/L at a pH 6.0. The adsorption capacity increases with increasing the concentration of $Li^+$ ions. The saturation values or monolayer coverage was achieved at an ion $Li^+$ concentration of 15 mmol/L and maximum adsorption capacities for $Fe_3O_4$@$SiO_2$@IIP (0.586 mmol/g) (Figure 3).

In order to analyze the $Li^+$ ions distribution between the bulk solution and $Fe_3O_4$@$SiO_2$@IIP and achieve the maximum adsorption uptake, Langmuir and Freundlich isotherm models were used to described the equilibrium data.

$$\text{Langmuir model: } Q_e = \frac{Q_m k_l C_e}{1 + k_l C_e}$$

$$\text{Freundlich model: } Q_e = K_f C_e^{1/n}$$

where $C_e$ (mmol $L^{-1}$) and $Q_e$ (mmol $g^{-1}$) are the concentration and adsorbed amount of the $Li^+$ ion at adsorption equilibrium, respectively; $k_l$ is the Langmuir constant (L $mmol^{-1}$); $K_f$ is the Freundlich constant ($mmol^{1-(1/n)}$ $L^{1/n}$ $g^{-1}$); and $Q_m$ is the maximum adsorption capacity (mmol $g^{-1}$).

Table 1 and Figure S4 of the Supporting Information show the fitted constants of the Langmuir and Freundlich isotherms. We compared the values of the correlation coefficient ($R^2$) for the Langmuir with Freundlich isotherm, and the Langmuir model is better than the Freundlich model in describing the adsorption process, indicating that the sorption sites are basically homogeneous. As shown in Table S2 of the Supporting Information, the adsorption capacity of $Fe_3O_4$@$SiO_2$@IIP is higher than those reported in the literature.[36−39]

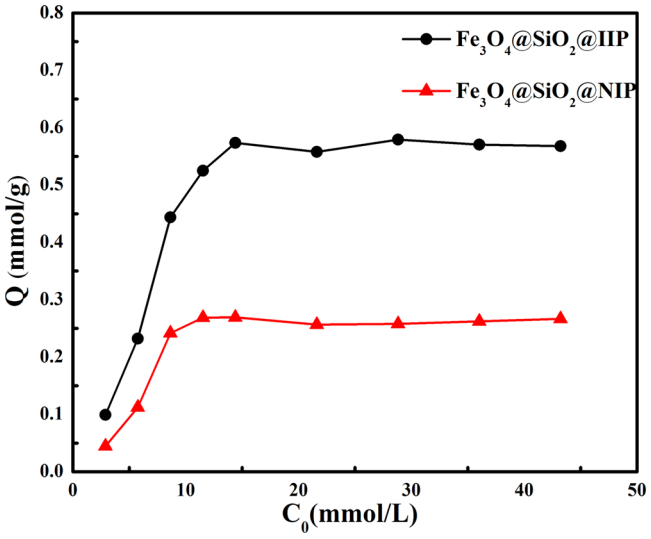


**Figure 3.** $Li^+$ ion adsorption isotherms for $Fe_3O_4$@$SiO_2$@IIP and $Fe_3O_4$@$SiO_2$@NIP. Conditions: 50 mg of sorbent, 50 mL of Li(I), and temperature of 25 °C.

*Absorption Kinetics.* Adsorption dynamics were carried out to evaluate the ionic transfer on $Fe_3O_4$@$SiO_2$@IIP and $Fe_3O_4$@$SiO_2$@NIP. The kinetic data shown in Figure 4 indicates that the absorption of $Li^+$ increased rapidly within 5 min, followed by a relatively slow process, and then the sorption equilibrium was achieved within 10 min. In addition, no remarkable changes were observed from 10 to 60 min.

In order to study the mechanism of the adsorption kinetics, the pseudo-second-order rate equation and the mass flow rate equation were employed to describe the adsorption kinetics of $Li^+$ ions on $Fe_3O_4$@$SiO_2$@IIP and $Fe_3O_4$@$SiO_2$@NIP. The pseudo-second-order equation is given as follows

$$\frac{t}{Q_t} = \frac{1}{K_2 \times Q_e^2} + \frac{1}{Q_e} \times t$$

$$h_0 = K_2 \times Q_e^2$$

where $Q_e$ and $Q_t$ are the amount of $Li^+$ ion adsorbed at adsorption equilibrium and any time, respectively (mmol $g^{-1}$); $K_2$ is the adsorption constant ($min^{-1}$); and $h_0$ is the initial adsorption rate (g $mmol^{-1}$ $min^{-1}$).

The mathematical derivation process of the mass flow rate equation on $Fe_3O_4$@$SiO_2$@IIP is shown in section S4 of the Supporting Information. The mass flow rate equation is given as follows

$$-\frac{dC}{dt} = k_f \times a(C - C_s)$$

$$C = b \exp[-ht] + C_0 - b$$

where $C$ is the concentration of $Li^+$ (mmol/L) in bulk solution at any time $t$; $C_s$ is the concentration of $Li^+$ at interface (mmol/L); $h$ and $b$ are the fitting parameters; and $k_f$ is the mass transfer coefficient (m/s).

The regression data fitted to the pseudo-second-order equation are shown in Figure S5 of the Supporting Information, and the related kinetics constants and regression values are summarized in Table 2. The correlation coefficients ($R^2$) of


DOI: 10.1021/sc500659h
ACS Sustainable Chem. Eng. 2015, 3, 460−467

**Table 1. Langmuir and Freundlich Adsorption Isotherm Constants for $Li^+$ ion on $Fe_3O_4$@$SiO_2$@IIP and $Fe_3O_4$@$SiO_2$@NIP**

| | Langmuir | | | | Freundlich | | |
|---|---|---|---|---|---|---|---|
| adsorbent | $Q_{max,cal}$ (mmol $g^{-1}$) | $Q_{max,exp}$ (mmol $g^{-1}$) | $k_l$ (L $mmol^{-1}$) | $R^2$ | $n$ | $K_f$ ($(mmol^{1-(1/n)}$ $L^{1/n}$ $g^{-1}$) | $R^2$ |
| IIP | 0.596 | 0.58 | 0.64 | 0.998 | 0.784 | 42.85 | 0.687 |
| NIP | 0.266 | 0.26 | 2.42 | 0.995 | 0.848 | 95.94 | 0.607 |

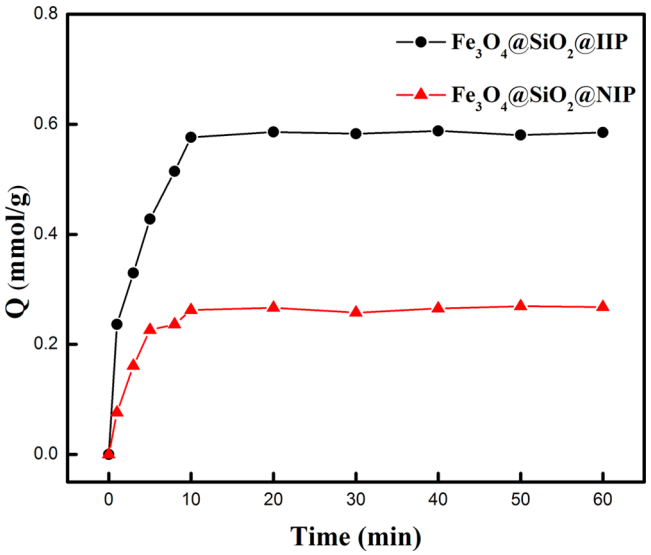


**Figure 4.** Adsorption kinetics for $Li^+$ ion adsorption on $Fe_3O_4$@$SiO_2$@IIP and $Fe_3O_4$@$SiO_2$@NIP. Conditions: 100 mg of sorbent, 200 mL of Li(I), concentration of 10 mmol/L, and temperature of 25 °C.

**Table 2. Kinetic Parameters of Pseudo-Second-Order Rate Equation for $Li^+$ Adsorption on $Fe_3O_4$@$SiO_2$@IIP and $Fe_3O_4$@$SiO_2$@NIP**

| sorbents | $K_2$ | $Q_e$ | $h_0$ | $R^2$ |
|---|---|---|---|---|
| $Fe_3O_4$@$SiO_2$@IIP | 1.29 | 0.595 | 0.458 | 0.9989 |
| $Fe_3O_4$@$SiO_2$@NIP | 2.36 | 0.276 | 0.180 | 0.9986 |

$Fe_3O_4$@$SiO_2$@IIP and $Fe_3O_4$@$SiO_2$@NIP are 0.9989 and 0.9986, respectively. The $Q_e$ (0.595 mmol/g) parameter for the pseudo-second-order equation is also close to the experimental result (0.586 mmol/g). Moreover, the initial adsorption rate $h_0$ of $Fe_3O_4$@$SiO_2$@IIP is higher than that of $Fe_3O_4$@$SiO_2$@NIP, which is probably due to imprinted effect and strong affinity between Li ions and imprinted polymer structures. The results indicate that the pseudo-second-order mechanism is primary and that the potential rate-controlling step in $Li^+$ absorption was chemical absorption.

Figure 5 shows the data fitted with the mass transfer model. The mass transfer coefficient and nonlinear regression values are summarized in Table 3. The obtained $R^2$ values of $Fe_3O_4$@$SiO_2$@IIP and $Fe_3O_4$@$SiO_2$@NIP are 0.974 and 0.995, respectively. The obtained parameter of $Fe_3O_4$@$SiO_2$@NIP (5.56 × 10−4 m/s) is higher than that of $Fe_3O_4$@$SiO_2$@IIP (5.14 × $10^{-4}$ m/s), which can be attributed to the steric hindrance effect caused by the imprinted cavity. The obtained $k_l$ and $Q_m$ values in $Fe_3O_4$@$SiO_2$@IIP and $Fe_3O_4$@$SiO_2$@NIP are almost same as those from Langmuir model. These results verified that the mass flow rate equations are suitable for explaining the adsorption kinetics.

*Adsorption Selectivity.* The selectivity of $Fe_3O_4$@$SiO_2$@IIP toward the Li(I) ion was studied by competitive adsorption in

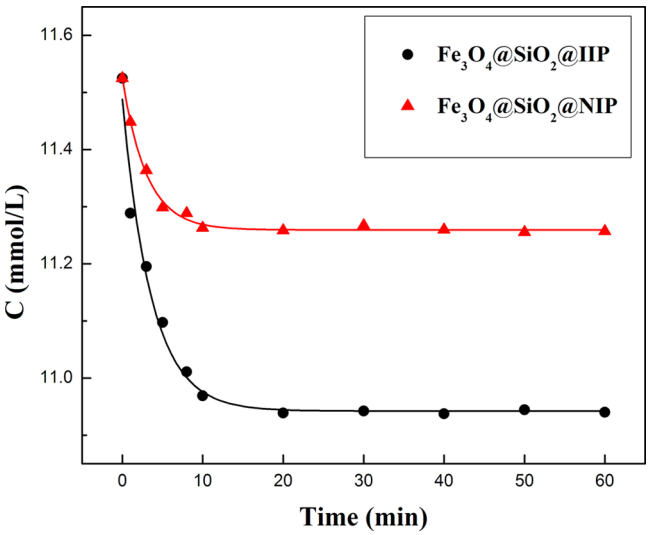


**Figure 5.** Nonlinear plot of $C$ vs $t$ for $Fe_3O_4$@$SiO_2$@IIP and $Fe_3O_4$@$SiO_2$@NIP.

**Table 3. Kinetic Parameters of Mass Flow Rate Equation for $Li^+$ Adsorption on $Fe_3O_4$@$SiO_2$@IIP and $Fe_3O_4$@$SiO_2$@NIP**

| sorbents | $k_f$ (m/s) | $k_l$ (L/mmol) | $Q_m$ (mmol $g^{-1}$) | $R^2$ |
|---|---|---|---|---|
| $Fe_3O_4$@$SiO_2$@IIP | 5.14 × $10^{-4}$ | 0.61 | 0.59 | 0.974 |
| $Fe_3O_4$@$SiO_2$@NIP | 5.56 × $10^{-4}$ | 2.08 | 0.27 | 0.995 |

the presence of Na(I), K(I), Cu(II), and Zn(II) ions and the individual initial concentration of 100 mg/L. After a competitive adsorption equilibrium, the concentrations of Li(I), Na(I), K(I), Cu(II), and Zn(II) in the remaining samples were determined by FAAS. The selectivity separation factor of Li(I) with respect to other ions ($\alpha_M^{Li}$) and the relative selectivity separation factor ($\alpha_r$) were calculated by following equations.[36]

$$\alpha_M^{Li} = \frac{Q_{Li} C_M}{C_{Li} Q_M}$$

$$\alpha_r = \frac{\alpha_M^{Li}|_i}{\alpha_M^{Li}|_n}$$

$Q_{Li}$ and $Q_M$ represent the adsorption capacity (equiv/gram) of sorbent toward Li(I) and other ions, respectively; $C_{Li}$ and $C_M$ represent the ion concentration (equiv/L) of Li(I) and other ions, respectively; and $\alpha_M^{Li}|_i$ and $\alpha_M^{Li}|_n$ represent the selectivity factor separation of $Fe_3O_4$@$SiO_2$@IIP and $Fe_3O_4$@$SiO_2$NIP, respectively.

Na(I) and K(I) are chosen as the competitor ions due to the same charge, while Cu(II) and Zn(II) are selected because of their similar ionic radius (ionic radius: Cu (II), 71 pm; Zn (II), 74 pm; and Li (I), 76 pm). Figure 6 depicts the uptake of Li(I), Na(I), K(I), Cu(II), and Zn(II) ions by $Fe_3O_4$@$SiO_2$@IIP and NIP. $Fe_3O_4$@$SiO_2$@IIP exhibits much larger adsorption


DOI: 10.1021/sc500659h
ACS Sustainable Chem. Eng. 2015, 3, 460−467

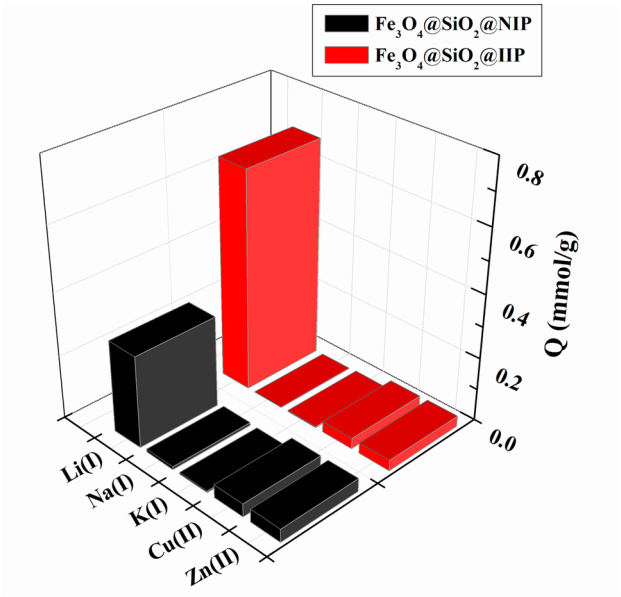


**Figure 6.** Selective binding analysis of $Li^+$ ion by $Fe_3O_4$@$SiO_2$@IIP and $Fe_3O_4$@$SiO_2$@NIP. Conditions: 50 mg of sorbent, 50 mL of Li(I), concentration of 10 mmol/L, and temperature of 25 °C.

capacity for Li(I) than other ions. Furthermore, $Fe_3O_4$@$SiO_2$@IIP and $Fe_3O_4$@$SiO_2$@NIP particles exhibit very low adsorption capacity for Na(I) and K(I), and the adsorption capacities for Cu(II) and Zn(II) were relatively low compared with Li(I). The above results can be attributed to the specific selective recognition ability of $Fe_3O_4$@$SiO_2$@IIP for Li(I).

Selectivity separation factor and relative selectivity separation factor were summarized in Table 4. As shown in Table 4, the

**Table 4. Selectivity Parameters of Adsorbents for $Fe_3O_4$@$SiO_2$@IIP and $Fe_3O_4$@$SiO_2$@NIP**

| metal ions | $Fe_3O_4$@$SiO_2$@IIP ($\alpha^{Li}_{M^+_i}$) | $\alpha_r$ | $Fe_3O_4$@$SiO_2$@NIP ($\alpha^{Li}_{M^+_n}$) |
|---|---|---|---|
| Na(I) | 50.88 | 4.92 | 10.33 |
| K(I) | 42.38 | 4.10 | 10.33 |
| Cu(II) | 22.5 | 3.34 | 6.7 |
| Zn(II) | 22.2 | 3.04 | 7.3 |

selectivities of Li(I) with respect to Na(I), K(I), Cu(II), and Zn(II) in $Fe_3O_4$@$SiO_2$@IIP are greater than 22 for the imprinted crown ether. The relative selectivity of $Fe_3O_4$@$SiO_2$@IIP as compared to that of $Fe_3O_4$@$SiO_2$@NIP is greater than 3.0. Accordingly, Li(I) fits better into the imprinted cavities and has a higher affinity with the crown ether groups than Na(I), K(I), Cu(II), and Zn(II).

*Regeneration.* The regeneration of the adsorbent is an economic factor to evaluate the practical performance of adsorbent, which is the reusability and stability of $Fe_3O_4$@$SiO_2$@IIP. $Fe_3O_4$@$SiO_2$@IIP was subject to five adsorption−desorption cycles, and the results are shown in Figure S6 of the Supporting Information. The capacity for Li(I) decreases slightly after each regeneration, and the adsorption capacity of $Fe_3O_4$@$SiO_2$@IIP in the fifth adsorption−desorption cycle for $Li^+$ was 92.4% of that in the first cycle. The results show that $Fe_3O_4$@$SiO_2$@IIP has excellent regeneration efficiency.

*Fixed-Bed Column Experiments.* In order to confirm the applicability of $Fe_3O_4$@$SiO_2$@IIP for the removal of Li(I) ions in real water samples, fixed-bed column experiments were investigated. Wastewater (Dingxin Co., Ltd., Shangrao China) was selected and analyzed. The composition of the wastewater is listed in Table S1 of the Supporting Information. The wastewater contains large amounts of heavy metals (Li, K, Zn, Co, Cr, Cu, Al, Ni, Pb, and Cd), and the pH value of the wastewater is 9.2. Figure 7 shows the breakthrough curves of

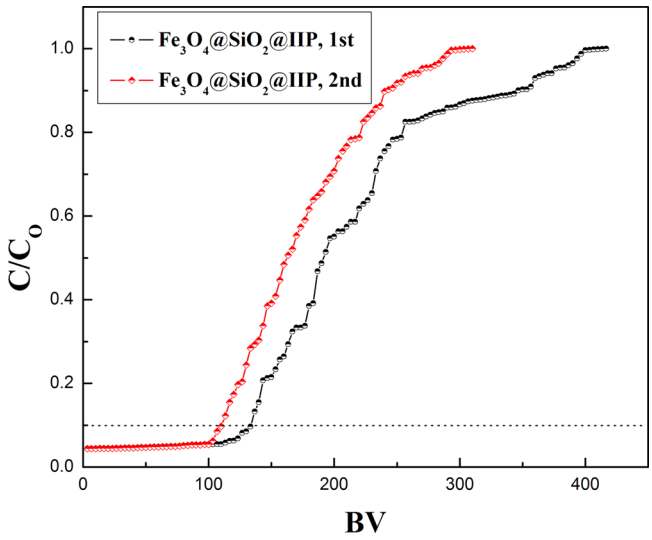


**Figure 7.** Fixed-bed column adsorption test.

$Fe_3O_4$@$SiO_2$@IIP toward the $Li^+$ ion. For $Fe_3O_4$@$SiO_2$@IIP, the effective treatment volume was 140 BV for the first run when the breakthrough was fixed at 10% of the inlet concentration, and 110 BV was achieved for the second run under identical conditions, suggesting that $Fe_3O_4$@$SiO_2$@IIP exhibited a stable performance for $Li^+$ ion removal. The exhausted $Fe_3O_4$@$SiO_2$@IIP column was subsequently regenerated in situ with the HCl solution (0.5 mol/L), and then the desorption equilibrium was achieved within 2 BV. No leaching of $Fe_3O_4$ was observed during the cyclic adsorption runs by detecting the Fe content in effluent.

In addition, the cumulative desorption efficiency was around 89.9% for the first run and ~98.7% for the second run (Figure 8). About 10% of the $Li^+$ ion absorbed by the fresh $Fe_3O_4$@$SiO_2$@IIP could not be effectively desorbed by 0.5 mmol/L HCl solution, which may due to the chelation of $Fe_3O_4$@$SiO_2$@IIP on the $Li^+$ ion even under the condition of pH 0.3. Moreover, to further explain this phenomenon, the pH (pH 0.3, 3, 6) effect on adsorption capacity was investigated and is shown in Figure S7 of the Supporting Information. The adsorption capacities, $Q$, in pH 0.3 (0.06 mmol/g) and pH 3 (0.46 mmol/g) are only about 10% and about 80% of the $Q_m$ in pH 6 (0.58 mmol/g), respectively. This evidence verifies the above assumption and may infer that about 10% of the $Li^+$ ion absorbed by the fresh $Fe_3O_4$@$SiO_2$@IIP could not be effectively desorbed by 0.5 mol/L HCl solution.

To prepare Li chemical materials removed from wastewater, the desorption solutions in fixed-bed experiments were heated and flash evaporated, and then 104 mg of the product was obtained. The product was analyzed by ion chromatography and AAS. The results demonstrate that the product is lithium chloride, with a content of 96.48%. Few impurities in the lithium chloride also verified strongly that $Fe_3O_4$@$SiO_2$@IIP is a highly selective material for Li ions and can effectively recycle


DOI: 10.1021/sc500659h
ACS Sustainable Chem. Eng. 2015, 3, 460−467

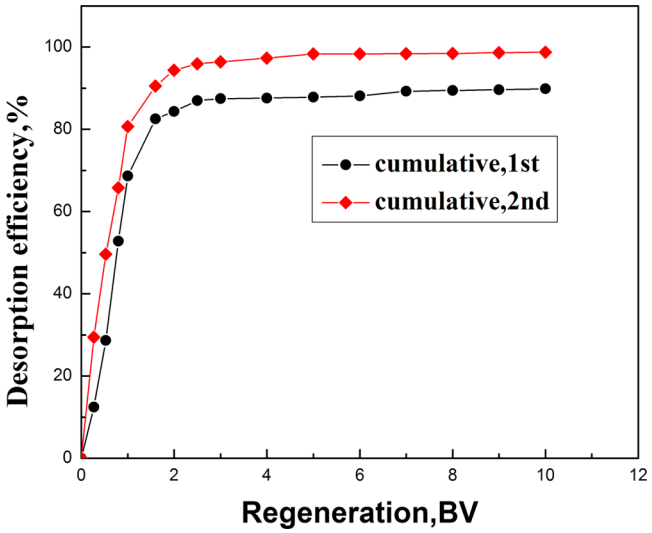


**Figure 8.** Fixed-bed column regeneration test.

Li ions from the complex wastewater. When one ton of the wastewater is treated in this way, 15.4 L of desorption solution was produced, and the concentration of Li(I) can be enriched 55 or 70 times. A total of 4.3 kg of white lithium chloride was collected after the solution was flash evaporated. The recovery of Li creates ¥240.8 economic value for enterprises (according to the lowest price 56 ¥/kg).

**Conclusions.** In summary, this study developed an effective material to recycle Li(I) ions from wastewater through a surface-imprinting technique using 2-(allyloxy)methyl-12-crown-4 as a functional monomer. The as-prepared $Fe_3O_4$@$SiO_2$@IIP combined high adsorption ability and excellent selectivity for Li(I) ions with rapid external mass transfer coefficients ($k_f = 5.56 \times 10^{-4}$ m/s). This guaranteed that it can remove and recycle Li(I) ions from real wastewater. When one ton of the wastewater is treated in this way, 4.3 kg of white lithium chloride is recycled, which creates ¥240.8 economic interest for enterprises. If the low cost and long service life of the magnetic lithium ion-imprinted polymers are realized, magnetic lithium ion-imprinted polymers would have a promising place in the large-scale application of treating industrial wastewater produced by spent lithium battery recycling enterprises in the future.

## ■ ASSOCIATED CONTENT

### Supporting Information

Details about chemicals, characterization methods, preparation of MH-$Fe_3O_4$@$SiO_2$, mathematical derivation process of the mass flow rate equation, SEM and XRD photographs, effect of pH in absorption tests, regeneration, and basic properties of real wastewater. This material is available free of charge via the Internet at http://pubs.acs.org.

## ■ AUTHOR INFORMATION

### Corresponding Authors

*Tel: +86 73183953371. Fax: +86 73183953373. E-mail: sllou@hnu.edu.cn.

*Tel: 404-894-7895. E-mail: john.crittenden@ce.gatech.edu.

### Notes

The authors declare no competing financial interest.

## ■ ACKNOWLEDGMENTS

This work was financially supported by the Natural Science Foundation of China (51178213, 51238002, 51272099, and 51308278), National Science Fund for Excellent Young Scholars (51422807), and Program for New Century Excellent Talents in University (NCET-11-1004).

## ■ REFERENCES

(1) Granata, G.; Moscardini, E.; Pagnanelli, F.; Trabucco, F.; Toro, L. Product recovery from Li-ion battery wastes coming from an industrial pre-treatment plant: Lab scale tests and process simulations. *J. Power Sources* **2012**, *206*, 393−401.

(2) Li, L.; Lu, J.; Ren, Y.; Zhang, X. X.; Chen, R. J.; Wu, F.; Amine, K. Ascorbic-acid-assisted recovery of cobalt and lithium from spent Li-ion batteries. *J. Power Sources.* **2012**, *218*, 21−27.

(3) Niu, Z. R.; Zou, Y. K.; Xin, B. P.; Chen, S.; Liu, C. H.; Li, Y. P. Process controls for improving bioleaching performance of both Li and Co from spent lithium ion batteries at high pulp density and its thermodynamics and kinetics exploration. *Chemosphere.* **2014**, *109*, 92−98.

(4) Sun, L.; Qiu, K. Q. Vacuum pyrolysis and hydrometallurgical process for the recovery of valuable metals from spent lithium-ion batteries. *J. Hazard Mater.* **2011**, *194*, 378−384.

(5) Wang, R. C.; Lin, Y. C.; Wu, S. H. A novel recovery process of metal values from the cathode active materials of the lithium-ion secondary batteries. *Hydrometallurgy.* **2009**, *99*, 194−201.

(6) Li, L.; Ge, J.; Chen, R. J.; Wu, F.; Chen, S.; Zhang, X. X. Environmental friendly leaching reagent for cobalt and lithium recovery from spent lithium-ion batteries. *Waste Manage.* **2010**, *30*, 2615−2621.

(7) Sun, L.; Qiu, K. Q. Vacuum pyrolysis and hydrometallurgical process for the recovery of valuable metals from spent lithium-ion batteries. *J. Hazard Mater.* **2011**, *194*, 378−384.

(8) Shin, S. M.; Kim, N. H.; Sohn, J. S.; Yang, D. H.; Kim, Y. H. Development of a metal recovery process from Li-ion battery wastes. *Hydrometallurgy.* **2005**, *79*, 172−181.

(9) Ferreira, D. A.; Prados, L.M. Z.; Majuste, D.; Mansur, M. B. Hydrometallurgical separation of aluminium, cobalt, copper and lithium from spent Li-ion batteries. *J. Power Sources* **2009**, *187*, 238−246.

(10) Zhang, P. W.; Yokoyama, T.; Itabashi, O.; Toshishige, M.; Suzuki; Inoue, K. Hydrometallurgical process for recovery of metal values from spent lithium-ion secondary batteries. *Hydrometallurgy* **1998**, *47*, 259−271.

(11) Lupi, C.; Pasquali, M.; DellEra, A. Nickel and cobalt recycling from lithium-ion batteries by electrochemical processes. *Waste Manage.* **2005**, *25*, 215−220.

(12) Freitas, M. B. J. G.; Celante, V. G.; Pietre, M. K. Electrochemical recovery of cobalt and copper from spent Li-ion batteries as multilayer deposits. *J. Power Sources* **2010**, *195*, 3309−3315.

(13) Lemaire, J.; Svecova, L.; Lagallarde, F.; Laucournet, R.; Thivel, P. X. Lithium recovery from aqueous solution by sorption/desorption. *Hydrometallurgy* **2014**, *143*, 1−11.

(14) McKnight, R. F.; Adida, M.; Budge, K.; Stockton, S.; Goodwin, G. M.; Geddes, J. R. Lithium toxicity profile: A systematic review and meta-analysis. *Lancet* **2012**, *379*, 721−28.

(15) Ivkovic, A.; Stern, T. A. Lithium-induced neurotoxicity: Clinical presentations, pathophysiology, and treatment. *Psychosomatics* **2014**, *55*, 296−302.

(16) Yamaguchi, H.; Inoshita, M.; Shirakami, A.; Hashimoto, S.; Ichimiya, C.; Shigekiyo, T. A case of severe hypothyroidism causing cardiac tamponade associated with lithium intoxication. *J. Cardiol. Cases* **2013**, *8*, e42−e45.

(17) Tsuruta, T. Removal and recovery of lithium using various microorganisms. *J. Biosci. Bioeng.* **2005**, *100*, 562−566.

(18) Zhu, G.; Zhu, P.; Qi, P. F.; Gao, C. J. Adsorption and desorption properties of Li+ on PVC-$H_{1.6}Mn_{1.6}O_4$ lithium ion-sieve membrane. *Chem. Eng. J.* **2014**, *235*, 340−348.



DOI: 10.1021/sc500659h
*ACS Sustainable Chem. Eng.* 2015, 3, 460−467

(19) Lu, Y. K.; Yan, X. P. An imprinted organic-inorganic hybrid sorbent for selective separation of cadmium from aqueous solution. *Anal. Chem.* **2004**, *76*, 453−457.
(20) Singh, D. K.; Mishra, S. Synthesis, characterization and removal of Cd(II) using Cd(II)-ion imprinted polymer. *J. Hazard Mater.* **2009**, *164*, 1547−1551.
(21) Saraji, M.; Yousefi, H. Selective solid-phase extraction of Ni(II) by an ion-imprinted polymer from water samples. *J. Hazard Mater.* **2009**, *167*, 1152−1157.
(22) Xu, S. F.; Chen, L. X.; Li, J. H.; Guan, Y. F.; Lu, H. Z. Novel $Hg^{2+}$-imprinted polymers based on thymine−$Hg^{2+}$−thymine interaction for highly selective preconcentration of $Hg^{2+}$ in water samples. *J. Hazard Mater.* **2012**, *237*, 347−354.
(23) Hoai, N. T.; Yoo, D. K.; Kim, D. Batch and column separation characteristics of copper-imprinted porous polymer micro-beads synthesized by a direct imprinting method. *J. Hazard Mater.* **2010**, *173*, 462−467.
(24) Li, Z. C.; Fan, H. T.; Zhang, Y.; Chen, M. X.; Yu, Z. Y.; Cao, X. Q.; Sun, T. Cd(II)-imprinted polymer sorbents prepared by combination of surface imprinting technique with hydrothermal assisted sol-gel process for selective removal of cadmium(II) from aqueous solution. *Chem. Eng. J.* **2012**, *171*, 703−710.
(25) Guo, B.; Deng, F.; Zhao, Y.; Luo, X. B.; Luo, S. L.; Au, C. Magnetic ion-imprinted and −SH functionalized polymer for selective removal of Pb(II) from aqueous samples. *Appl. Surf. .Sci. .* **2014**, *292*, 438−446.
(26) Luo, X. B.; Luo, S. L.; Zhan, Y. C.; Shu, H. Y.; Huang, Y. N.; Tu, X. M. Novel Cu (II) magnetic ion imprinted materials prepared by surface imprinted technique combined with a sol−gel process. *J. Hazard Mater.* **2011**, *192*, 949−955.
(27) Wipff, G.; Weiner, P.; Kollman, P. A molecular mechanics study of 18-crown-6 and its alkali complexes: An analysis of structural flexibility, ligand specificity, and the macrocyclic effect. *J. Am. Chem. Soc.* **1982**, *82*, 1504−3249.
(28) Luo, X. B.; Liu, L. L.; Deng, F.; Luo, S. L. Novel ion-imprinted polymer using crown ether as a functional monomer for selective removal of Pb(II) ions in real environmental water samples. *J. Mater. Chem. A* **2013**, *1*, 8280−8286.
(29) Rajabi, H. R.; Shamsipur, M.; Pourmortazavi, S. M. Preparation of a novel potassium ion imprinted polymeric nanoparticles based ondicyclohexyl 18C6 for selective determination of $K^+$ ion in different water samples. *Mater. Sci. Eng. C* **2013**, *33*, 3374−3381.
(30) Shamsipur, M.; Rajabi, H. R. Flame photometric determination of cesium ion after its preconcentration with nanoparticles imprinted with the cesium-dibenzo-24-crown-8 complex. *Microchim Acta.* **2013**, *180*, 243−252.
(31) Peng, S.; Sun, S. H. Synthesis and characterization of monodisperse hollow $Fe_3O_4$ nanoparticles. *Angew. Chem.* **2007**, *199*, 4233−4236.
(32) Bao, J.; Chen, W.; Liu, T. T.; Zhu, Y. L.; Jin, P. Y.; Wang, L. Y.; Liu, J. F.; Wei, Y. G.; Li, Y. D. Bifunctional Au-$Fe_3O_4$ nanoparticles for protein separation. *ACS Nano* **2007**, *4*, 293−298.
(33) Yang, X. Y.; Zhang, X. Y.; Ma, Y. F.; Huang, Y.; Wang, Y. S.; Chen, Y. S. Superparamagnetic graphene oxide−$Fe_3O_4$ nanoparticles hybrid for controlled targeted drug carriers. *J. Mater. Chem.* **2009**, *19*, 2710−2714.
(34) Xie, B. J.; Xu, C. J.; Kohler, N.; Hou, Y. L.; Sun, S. H. Controlled PEGylation of monodisperse $Fe_3O_4$ nanoparticles for reduced non-specific uptake by macrophage cells. *Adv. Mater.* **2007**, *19*, 3163−3166.
(35) Zhang, M. L.; Zhang, Z. H.; Liu, Y. N.; Yang, X.; Luo, L. J.; Chen, J. T.; Yao, S. Z. Preparation of core−shell magnetic ion-imprinted polymer for selective extraction of Pb(II) from environmental samples. *Chem. Eng. J.* **2011**, *178*, 443−450.
(36) Crittenden, J. C.; Trussell, R. R.; Hand, D. W.; Howe, K. J.; Tchobanoglous, G. *MWH's Water Treatment: Principles and Design.* Wiley 2012.
(37) Umeno, A.; Miyai, Y.; Takagi, N.; Chitrakar, R.; Sakane, K.; Ooi, K. Preparation and adsorptive properties of membrane-type adsorbents for lithium recovery from seawater. *Ind. Eng. Chem. Res.* **2002**, *41*, 4281−4287.
(38) Han, Y.; Kim, H.; Park, J. Millimeter-sized spherical ion-sieve foams with hierarchical pore structure for recovery of lithium from seawater. *Chem. Eng. J.* **2012**, *210*, 482−489.
(39) Wang, L.; Ma, W.; Liu, R.; Li, H. Y.; Meng, C. G. Correlation between $Li^+$ adsorption capacity and the preparation conditions of spinel lithium manganese precursor. *Solid State Ionics.* **2006**, *177*, 1421−1428.
(40) Song, D.; Park, S.; Kang, H. W.; Park, S. B.; Han, J. Recovery of lithium(I), strontium(II), and lanthanum(III) using Ca-alginate beads. *J. Chem. Eng. Data* **2013**, *58*, 2455−2464.


DOI: 10.1021/sc500659h
*ACS Sustainable Chem. Eng.* 2015, 3, 460−467